Diffusion of Microspheres in Shear Flow Near a Wall: Use to Measure Binding Rates between Attached Molecules

Anne Pierres,* Anne-Marie Benoliel,* Cheng Zhu,† and Pierre Bongrand*
*Laboratoire d'Immunologie, Hôpital de Sainte-Marguerite, 13274 Marseille Cedex 09, France and †George W. Woodruff School of Mechanical Engineering, Georgia Institute of Technology, Atlanta, Georgia 30332 USA

ABSTRACT The rate and distance-dependence of association between surface-attached molecules may be determined by monitoring the motion of receptor-bearing spheres along ligand-coated surfaces in a flow chamber (Pierres et al., *Proc. Natl. Acad. Sci. U.S.A.* 95:9256–9261, 1998). Particle arrests reveal bond formation, and the particle-to-surface distance may be estimated from the ratio between the velocity and the wall shear rate. However, several problems are raised. First, data interpretation requires extensive computer simulations. Second, the relevance of standard results from fluid mechanics to micrometer-size particles separated from surfaces by nanometer distances is not fully demonstrated. Third, the wall shear rate must be known with high accuracy. Here we present a simple derivation of an algorithm permitting one to simulate the motion of spheres near a plane in shear flow. We check that theoretical predictions are consistent with the experimental dependence of motion on medium viscosity or particle size, and the requirement for equilibrium particle height distribution to follow Boltzman's law. The determination of the statistical relationship between particle velocity and acceleration allows one to derive the wall shear rate with 1-s^{-1} accuracy and the Hamaker constant of interaction between the particle and the wall with a sensitivity better than 10^{-21} J. It is demonstrated that the correlation between particle height and mean velocity during a time interval Δt is maximal when Δt is about 0.1–0.2 s for a particle of 1.4-μm radius. When the particle-to-surface distance ranges between 10 and 40 nm, the particle height distribution may be obtained with a standard deviation ranging between 8 and 25 nm, provided the average velocity during a 160-ms period of time is determined with 10% accuracy. It is concluded that the flow chamber allows one to detect the formation of individual bonds with a minimal lifetime of 40 ms in presence of a disruptive force of ~5 pN and to assess the distance dependence within the tens of nanometer range.

GLOSSARY

a = sphere radius
A_H = Hamaker constant for the sphere-to-plane interaction in liquid medium
c = local particle concentration
D^0 = diffusion coefficient at distance from the surface
D_x, D_z = components of the diffusion matrix parallel to the x and z axis, respectively
$D_{\omega y}$ = rotational diffusion coefficient around axis Oy
f_+, f_- = probability of upward and downward jump of length l during an elementary time interval
F_x, F_z = dimensionless damping coefficient for diffusion of a sphere near a surface along axis x and z, respectively
F^R, F^{*R} = force and dimensionless force coefficient applied by the fluid on a sphere rotating near a wall with fixed center.
F^T, F^{*T} = force and dimensionless force coefficient applied by the fluid on a sphere moving without rotation parallel to a wall
k_B = Boltzmann constant
g = gravity acceleration
G = wall shear rate
h = height of the chamber channel
h_B = average z coordinate of a buoyant Brownian particle sedimenting on a surface
J = diffusive current
l = elementary step used to simulate diffusion along the z coordinate
n_i = number of particles at distance $(2i + 1)l/2$ from the surface
$P_{U,\Delta t}(z)$ = probability density of coordinate z for a particle with average translation velocity U during Δt
Q = flow rate

Received for publication 7 August 2000 and in final form 2 April 2001.

Present address: Pierre Bongrand, Hopital de Sainte-Marguerite, INSERM U 387, Lab d'Immunologie, BP 29, 13274 Marseille Cedex 09, France. Tel.: +33-491-26-03-31; Fax: +33-491-75-73-28; E-mail: bongrand@marseille.inserm.fr.

0006-3495/01/07/25/18 $2.00

R = random displacement of a sphere along Ox
T = absolute temperature
T^R, T^{*R} = torque and dimensionless torque coefficient applied by the fluid on a sphere rotating near a wall with fixed center
T^T, T^{*T} = torque and dimensionless torque coefficient applied by the fluid on a sphere moving without rotation parallel to a wall
u = instantaneous sphere velocity
u_B = contribution of brownian motion to the instantaneous sphere velocity
u_h = local hydrodynamic velocity of a sphere along x axis, in absence of diffusion
U = average sphere velocity (during time interval Δt)
U_B = contribution of Brownian motion to the average sphere velocity (during time interval Δt)
U_0 = average horizontal velocity (during time Δt) of particles when average acceleration is zero
v_s, v_s^0 = sedimentation velocity (local and at distance from the plane respectively)
V = theoretical fluid velocity at the sphere center
w = width of the chamber channel
$W(R)$ = distribution function for random displacement R
x = coordinate of the sphere center parallel to the fluid flow
z = coordinate of the sphere center perpendicular to the shear plane
γ_x = sphere acceleration along axis Ox
δ = distance between the sphere surface and plane
μ = medium viscosity
ρ = sphere density
ρ_w = medium density
Ω = sphere angular velocity

INTRODUCTION

Rates of adhesion and detachment are generally accepted as key determinants of cell adhesion mediated by receptor–ligand interactions, especially in a dynamic flow environment (Pierres et al., 1998a, Zhu 2000). Indeed, the critical step of cell adhesion may well be the formation of a first bond between ligand and receptor molecules borne by neighboring membranes. This first interaction might then transiently maintain membranes at binding distance and facilitate the formation of an increasing number of molecular interactions, thus stabilizing attachment (Pierres et al., 1998a). The outcome of the encounter should thus be highly dependent on the relative values of the dissociation rate of the first bond and the frequency of formation of additional links.

While the increasing development of surface plasmon resonance technology and availability of soluble forms of adhesion receptors renewed the interest of the biological community in the determination of the kinetic constants of association between these molecules (van der Merwe et al., 1993; Labadia et al., 1998; Boniface et al., 1999; Wilcox et al., 1999), the relevance of this recent experimental approach to cell interactions is difficult to assess. Indeed, in addition to the intrinsic difficulty of interpreting experimental data (Nieba et al., 1993; Schuck, 1997), the so-called three-dimensional (3D) kinetic rates measured with this technique should be quite different from their two-dimensional (2D) counterparts, namely those of binding between membrane-bound molecules (Bell, 1978).

Thus, bonds formed between membrane molecules are often forced to dissociate (or ruptured by force) when cells are brought apart, which makes the off-rate k_{off} a function of force (instead of a mere constant as in the 3D case—see Bell, 1978). A relatively straightforward technique has recently been developed for measuring the force dependence of 2D k_{off}, which is derived from the statistics of duration of the transient tethering of moving cells to a stationary surface in the flow chamber (Kaplanski et al., 1993; Pierres et al., 1995; Alon et al., 1995, 1997; Chen et al., 1997; Chen and Springer, 1999; Ramachandran et al., 1999; Smith et al., 1999). There are reports suggesting that values of the 2D k_{off} extrapolated to zero force measured by the flow chamber are comparable to the 3D k_{off} measured with biosensors (Pierres et al., 1996a; Mehta et al., 1998), both of which have the same unit of s^{-1}.

By contrast, the 2D k_{on} has a completely different dimension from, and hence cannot be directly compared to, the 3D k_{on} (in $M^{-1}s^{-1}$). Indeed, this 2D k_{on} is often expressed in $\mu m^2 s^{-1}$ (Dustin et al., 1996) and it was recently suggested (Pierres et al., 1996b, 1998b) that the most intrinsic parameter might be the frequency of bond formation between single ligand and receptor molecules maintained at distance d as a function of parameter d. This function $k_{on}(d)$ (in s^{-1}) is expected to depend on molecular properties such as length and flexibility (Pierres et al., 1998b). Also, a major physical reason underlying the difference between 2D and 3D k_{on} is that, instead of approaching each other by free

diffusion as in the 3D case, membrane adhesion molecules are brought together (and apart) by the cells to which they are anchored. Cells are 1000 times the size of the molecules, and, thereby, their motion dictates molecule transport before (and after) their intrinsic binding.

The experimental determination of $k_{on}(d)$ is fraught with considerable difficulty. The basic principle should consist of repeatedly bringing a receptor molecule and its ligand within binding distance with at least nanometer accuracy, then waiting for a well controlled period of time, and determining whether association occurred. Therefore, it is not surprising that there are only a few reports on the rate of bond formation between surface-attached molecules.

Several authors measured the frequency of bond formation between receptor-bearing surfaces and ligand-coated tips of atomic force microscopes (Hinterdorfer et al., 1996; Fritz et al., 1998; Baumgartner et al., 2000). Estimating the binding range on the basis of molecular size, they were able to derive an average association rate. However, this approach did not yield any information on the distance-dependence of binding frequency.

Chesla et al. (1998) used micropipettes driven by a piezoelectric translator to control repeated contacts between receptor-expressing cells (see also Chesla et al., 2000; Williams et al., 2000a & b). This method should, in principle, allow for fairly direct determination of the 2D kinetic rates from the measured dependence of adhesion frequency on contact time. However, it is necessary to establish the relevance of these parameters, which are estimated from adhesions over contact times ranging from subsecond to 10+ seconds, to those that govern the leukocyte tethering to and rolling on endothelial cells in a shear flow, which occurs in millisecond encounter duration. Also, no information can be obtained via this approach regarding the dependence of 2D on-rate on the separation distance between the two cells, which have impinged onto each other.

Pierres et al. (1997, 1998c, d) observed the motion of ligand-coated spheres driven along receptor-derivatized surfaces in presence of a hydrodynamic force low enough ($\sim$1 pN) to allow a single molecular bond to induce a detectable particle arrest. Because the sphere-to-surface distance could, in principle, be derived from the particle velocity with nanometer resolution (Pierres et al., 1997) and Brownian fluctuations made the particle-to-surface distance sample an interval of $\sim$100 nm, the function $k_{on}(d)$ should be derived from the statistics of binding frequency versus particle velocity. Also, because the relative velocity between interacting surfaces was of an order of several tens of micrometer per second, the duration of interactions between adhesion molecules of a few tens of nanometers fell into the millisecond range. This allowed better temporal resolution than atomic force microscopy (Fritz et al., 1998). However, experimental implementation of this idea has been tempered by a number of difficulties.

The main problem is that quantitative interpretation of binding frequencies is strongly dependent on the derivation of a relationship between particle velocity and distance to the surface. This is by no means trivial. 1) This derivation was based on numerical results obtained with basic principles of fluid mechanics. Although many authors have applied low Reynolds number hydrodynamics (Goldman et al., 1967a,b; Happel and Brenner, 1991) to model the motion of cells near the flow chamber floor, the validity of such theory has not been established when the particle-to-surface distance is as low as a few nanometers, which is comparable to the scale of surface roughness in many cases. 2) The aforementioned equations did not account for the Brownian motion of the sphere near the surface. This motion is quite difficult to describe with standard diffusion equations. Indeed, the hydrodynamic interaction between the sphere and the chamber floor may decrease the component of the diffusion matrix vertical to the surface by a factor of $\geq$100, and the understanding of diffusion in inhomogeneous media raises difficult problems (thus, the conventional Langevin approach may become meaningless: van Kampen, 1981; Risken, 1989).

The aim of the present paper is threefold. First, we describe a simple reasoning yielding an algorithm permitting one to simulate the motion of Brownian spheres at nanometer distance from a plane under shear flow. Second, we present results of a set of experiments designed to test the validity of this algorithm. Third, extensive simulations are performed to assess the feasibility of obtaining a quantitative relationship between the rate of association between receptor-coated spheres and ligand-bearing surfaces and the particle-to-surface distance. It is concluded that a quantitative analysis of the motion of particles subjected to a wall shear rate of 10 s^{-1} with a spatial accuracy of $\sim$25 nm and a time resolution of 20 ms will allow one to obtain the wall shear rate with about 1 s^{-1} accuracy, the Hamaker constant for the sphere-to-surface interaction with better than 10^{-21} J sensitivity, and the sphere-to-surface distance probability distribution with a standard deviation ranging from 8 to 25 nm when the distance increases from 14 to 40 nm. The present work extends our previous studies on the same subject (Pierres et al. 1998c,d). For the reader's convenience, the basic experimental setup is sketched on Fig. 1.

PRINCIPLE OF THE METHOD

Receptor-coated spheres of micrometer-size radius a are driven along ligand-coated surfaces by a laminar shear flow with a wall shear rate G of order of 10 s^{-1}. An automatic tracking device allows continuous recording of the x coordinate of the sphere center. Particle arrests are detected by a computer-assisted procedure, yielding immediate derivation of a quantitative relationship between average velocity during an elementary time step Δt and arrest probability (i.e., proportion of steps with this velocity that are followed

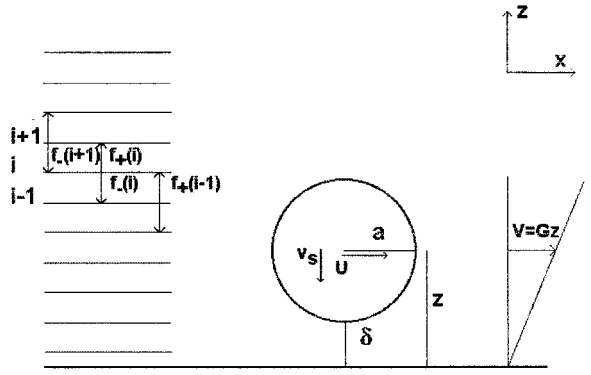

FIGURE 1 Model. The low Reynolds number motion of a sphere driven by a laminar shear flow near a plane is viewed as a linear combination of the following components: steady motion of a neutrally buoyant sphere according to Goldman et al. (1967a,b); sedimentation toward the plane, with a damping coefficient F_z due to the hydrodynamic interaction between the sphere and the surface; Brownian motion parallel to the plane, with damping coefficient F_x; vertical component of Brownian motion, with z-dependent damping coefficient F_z. The latter motion is simulated as a series of vertical jumps of fixed length, with a difference between the probabilities of upward and downward jump at any point.

by a detectable arrest). If the probability distribution of sphere-to-surface distance δ can be derived from the velocity, the binding probability of the sphere may be determined as a function of distance δ to the chamber floor. Finally, if the ligand and receptor densities on interacting surfaces are known, the frequency of intermolecular bond formation as a function of molecular distance can be derived by using a simple geometrical argument (Pierres et al., 1997).

The problem remains to calculate the probability distribution of parameter δ for a sphere of known average velocity during an elementary time step Δt. The aim of this paper is first to describe a suitable algorithm for deriving this probability distribution, second to provide an experimental check of the validity of the procedure, and third to discuss some consequences relevant to the experimental determination of binding rates.

THEORY

Let us consider a microsized buoyant sphere freely moving near a surface in presence of a laminar shear flow of shear rate G (Fig. 1). The instantaneous particle velocity is the sum of two contributions:

$$u = u_h + u_B. \tag{1}$$

u_h is the velocity component that may be described by a hydrodynamic process and is deterministically related to the shear rate and sphere-to-surface distance. u_B represents Brownian motion and must be treated as a random variable. We define U as the average velocity projected along the flow direction during a time interval Δt. We define $P_{U,\Delta t}(z)dz$ as the average fraction of time interval Δt during which the vertical coordinate of the particle center ranges beween z and $z + dz$, given the average velocity U during Δt. To define $P_{U,\Delta t}(z)$ also requires the a priori distribution of particle z coordinate. Because of the complexity of particle motion, our procedure for determining $P_{U,\Delta t}(z)$ consists of generating a representative ensemble of simulated particle trajectories and estimating $P_{U,\Delta t}(z)$ from their statistics.

Due to the choice of a low shear rate and micrometer-sized particles, the Reynolds number $Ga^2\rho_w/\mu$ (μ and ρ_w are the fluid viscosity and density, respectively) is very low (of order of 10^{-5}). This allows complete neglect of inertial effects and notably simplifies the flow properties (Happel and Brenner, 1991). Because flow equations are linear, instantaneous vertical and horizontal velocity components are independent. Indeed, if the displacement of the sphere parallel to the plane resulted in vertical upward force, reversal of the parallel displacement would result in reversal of the vertical force, which would be physically untenable. Thus, no first-order relationship can exist between horizontal and vertical motion. It is thus possible to treat vertical and horizontal displacements independently and simply superimpose them.

The motion parallel to the flow is represented as a sequence of elementary steps of duration Δt. The total displacement is the sum

$$\Delta x = u_h(\delta)\Delta t + R. \tag{2}$$

Here, $u_h(\delta)$ is the average velocity of a particle remaining at distance δ from the surface, and R is a Gaussian random variable accounting for particle diffusion parallel to the surface. Its distribution function $W(R)$ is (Ermak and McCammon, 1978; Rossky et al., 1978; Gabdouline and Wade, 1997; Evans and Ritchie, 1997)

$$W(R) = (1/4\pi D_x\Delta t)^{1/2}\exp(-R^2/4D_x\Delta t), \tag{3}$$

where D_x is the component of the diffusion matrix parallel to the flow. This may be written as

$$D_x = k_BT/6\pi\mu aF_x, \tag{4}$$

where k_B is Boltzmann's constant and T is the absolute temperature. $D^0 = k_BT/6\pi\mu a$ is the diffusion coefficient of a sphere of radius a in a boundless Newtonian fluid of viscosity μ. F_x is a dimensionless damping coefficient accounting for the presence of the wall. The influence of rotation on translational diffusion was neglected. As discussed in the Appendix, the error on D_x is expected to be lower than ~8%. Now, u_h and F_x may be expressed as functions of the dimensionless sphere-to-surface distance δ/a using a cubic approximation of numerical results provided by Goldman et al. (1967a,b), as displayed on Fig. 2,

$$u_h/aG = \exp(0.0037644[\ln(\delta/a)]^3 + 0.072332[\ln(\delta/a)]^2 + 0.54756[\ln(\delta/a)] + 0.68902), \tag{5}$$

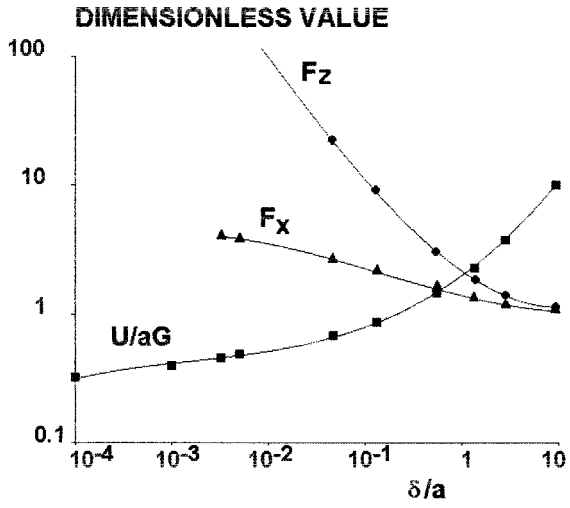

FIGURE 2 Steady motion of a sphere driven by a laminar shear flow near a plane. Numerical results from Goldman et al. (1967) are shown for the damping coefficients F_z (*circles*) and F_x (*triangles*), and dimensionless velocity U/aG (*squares*). These data were interpolated with cubic polynoma obtained by least square fit (*continuous lines*).

$$F_x = \exp(0.00332[\ln(\delta/a)]^3 + 0.019251[\ln(\delta/a)]^2 - 0.18271[\ln(\delta/a)] + 0.32747). \quad (6)$$

The motion perpendicular to the plane cannot be simulated in the same way because the diffusion coefficient is dependent on the z coordinate. If the hydrodynamic interaction between the sphere and the wall is accounted for by using a spatially varying diffusion coefficient, the Langevin-type approach exemplified by Eq. 1 becomes meaningless because it is not known which values must be used for D. Is it the diffusion coefficient at the beginning, the end, or even the middle of the elementary displacement? (van Kampen, 1981; Risken, 1989). This question is not trivial, because, although it may seem counter-intuitive, the differences resulting from different choices actually will not vanish as Δt becomes indefinitely small. Indeed, as shown below (Fig. 8 *A*), if one uses the diffusion coefficient at the starting point of any step (as suggested by Itô, see van Kampen, 1981 and Risken, 1989), the equilibrium distribution of the particle will differ from Boltzmann's distribution. This is obviously in contradiction with basic thermodynamic principles. (P.B. is indebted to Dr. Jacques Prost for introducing him to this difficulty, that is known as the Itô-Stratonovich dilemma.)

The reason for this problem may be explained as follows. If the diffusion coefficient is to be evaluated at the beginning of the step transition, a particle at height z would have a greater probability to move downward to $z - \Delta z$ than a particle at $z - \Delta z$ to move upward to z because $D_z(z) > D_z(z - \Delta z)$ [assuming that Δz is positive]. Conversely and for the very same reason, if the diffusion coefficient is to be evaluated at the end of the step transition, then the probability for a particle to move downward from above would be smaller than for a particle to move upward from below. These conclusions hold for all z values and arbitrarily small step size, and hence would result in particle concentration at the chamber floor in the former case, and in the mid-plane of the flow chamber in the latter case, neither of which is Boltzmann distribution. An alternative argument is that the net exchange of Brownian particles between two neighboring layers should be zero for the system to be at thermodynamic equilibrium. However, evaluating the diffusion coefficient either at the beginning or the end of the step transition would lead to a downward or upward net particle flux.

A reported way of dealing with this problem consists of adding a drift $\nabla D \cdot \Delta t$ to the particle displacement in Eq. 3 (Ermak and McCamoon, 1978; Brune and Kim, 1994). Another tentative way of solving this dilemma would be to evaluate the diffusion coefficient in the middle of the step displacement. In practice, however, the step size is not known before it is simulated from a random number generator that requires the value of diffusion coefficient as input for its probability distribution. Our solution is to convert the stochastic process of normally distributed step size to an equivalent random walk process of constant step size l with random jump frequencies. The key idea of our simulation is to use different frequencies for upward and downward jumps. Thus, the sphere-to-surface distance δ was written as $(2i + 1)l/2$, where i is any positive integer. The motion was then fully defined by the choice of transition frequencies between neighboring positions.

In a homogenous medium, it is readily shown from known random-walk properties that the root mean square displacement during time t would be $(2ft)^{1/2}l$, where f is the jump frequency. Because this is also equal to $(2Dt)^{1/2}$, where D is the diffusion coefficient, f is related to D through the simple formula,

$$f = D/l^2. \quad (7)$$

Now, using different frequencies for upward and downward jumps, we define $f_+(i)$ and $f_-(i)$ as the respective frequencies for jumps from position i to positions $(i + 1)$ and $(i - 1)$. The requirement for thermodynamic equilibrium between positions i and $i + 1$ requires that

$$f_+(i) = f_-(i + 1) \quad (8)$$

for any position i. This amounts to using, for the diffusion coefficient, the value at the middle between departure and arrival at any step. This principle may also be used to simulate the vertical motion of a sphere subjected to an external force F. Using Einstein's relationship, the mean velocity imparted on particles is FD/k_BT, which may be accounted for with a jump frequency of FD/lk_BT. Further, the diffusion coefficient may be written as D^0/F_z. The damping coefficient F_z can be expressed by approximating

numerical results from Brenner (1961) supplemented with the limiting form obtained at short distance with lubrication theory (Dimitrov, 1983), a result that was tested experimentally (Georges et al., 1993),

$$F_z = \exp(0.0057685[\ln(\delta/a)]^3 + 0.092235[\ln(\delta/a)]^2 - 0.52669[\ln(\delta/a)] + 0.76952). \quad (9)$$

Parameters $f_+(i)$ and $f_-(i)$ were then equated to D^0/l^2F_z, using for δ the values il and $(i-1)l$, respectively. Thus, at each time step Δt, the vertical displacement Δz was determinated as a sum of three random processes: 1) upward jump with probability $f_+(i)\Delta t$, 2) downward jump with probability $f_-(i')\ \Delta t$ (i' is i or $i+1$ depending on the preceding step), and 3) downward jump with probability $v_s^0\ \Delta t/lF_z$, where v_s^0 is the sedimentation velocity at distance from the plane, which is readily calculated as $[(4/3)\pi a^3(\rho - \rho_w)g]/[6\pi\mu a]$, where g is the acceleration of gravity.

In some cases, a fourth term was added to account for van der Waals attraction between the sphere and the plane. Using Derjaguin approximation (Israelachvili, 1991), the attraction force is $A_H a/6\delta^2$, where A_H is Hamaker constant. The transition probability is thus $A_H\Delta t/36\pi\mu F_z l$.

Equivalence with standard diffusion equations and previously reported algorithms

Now, instead of considering a single particle, let us consider an assembly of diffusing spheres with n_i particles at position i. The variation Δn_i after an elementary time step is

$$\Delta n_i = [(n_{i-1} - n_i)f_-(i) - (n_i - n_{i+1})f_+(i) + v_s^0(n_{i+1}/F_z(i+1) - n_i/F_z(i))]\Delta t. \quad (10)$$

The limit of Eq. 10 when Δt and l vanish is easily obtained by replacing $\Delta n_i/\Delta t$ with $\partial n/\partial t$ and differences such as $n_i - n_{i-1}$ with their derivatives such as $l\partial n/\partial z$. We obtain

$$\partial n/\partial t = l\partial/\partial z[f_+ l\partial n/\partial z] - \partial(v_s^0 n/F_z)/\partial z. \quad (11)$$

Using Eq. 7, we obtain

$$\partial n/\partial t = \partial/\partial z[D\partial n/\partial z - nv_s^0/F_z]. \quad (12)$$

Thus, our simulation procedure is fully consistent with standard diffusion theory, and amounts to adding a drift velocity equal to $\partial D/\partial z$ to the random motion of particles (Ermak and McCammon, 1978; Brune and Kim, 1994).

EXPERIMENTAL PROCEDURES

Our basic apparatus was described in previous papers (Pierres et al., 1996a,b) and only essential features will be recorded.

Surfaces

Streptavidin-coated spheres (2.8- and 4.5-μm diameter, 1300-kg/m^3 density) were provided by Dynal (Dynal France, Compiègne, France). According to the supplier, binding sites were scattered in a layer of 6-nm thickness. The flow chamber floor was obtained by cleaving mica (Muskovite mica, Metafix, Montdidier, France), to obtain a smooth surface at the subnanometer level. In some experiments, surfaces were coated with biotinyl-gly$_{12}$his$_6$ peptide as previously described (Pierres et al., 1998d).

Flow chamber

The flow chamber was custom-made by Satim (Evenos, France). It was made of a plexiglas block bearing a cavity of $0.1 \times 0.6 \times 20$ mm^3 surrounded by a toric gasket. The floor was made of mica sheets that were maintained against the gasket with a screwed steel plate. The flow was generated with a 1-ml syringe mounted on an electric syringe holder (Razel, supplied by Bioblock, Illkirch, France). This apparatus was driven with an asynchronous electric motor ensuring smooth motion.

Most experiments were performed in phosphate buffered solution. In some cases, 6% dextran (500,000 MW, Pharmacia, Sweden) was added. Viscosity was thus increased sevenfold, as measured by monitoring the gravity-driven flow through a syringe needle (Benoliel et al., 1994).

The chamber was set on the stage of an inverted microscope bearing a custom-made plate allowing easy positioning. Observation was done with a video camera (we used either a standard STM-M 108CE videocamera, Sony, supplied by Bioblock, France, or an LHR 712 rapid videosystem (Lhesa, Cergy-Pontoise, France).

Image processing

Images were stored on videotapes and later processed with a PCVision+ real time digitizer (Imaging Technology, Bedford, MA, supplied by Imasys, Suresnes, France) mounted on a desk computer. The even and odd fields of each picture were separated, yielding 50 images per second with a standard videocamera, and a typical pixel size of 0.24 and 0.34 μm along the horizontal and vertical axis, respectively, with a 40× objective. A custom-made software written with assembly language allowed particle tracking with real-time determination of the coordinates of the image center of gravity and surface area. We also used a rapid videosystem yielding 50 interlaced pictures per second. Each picture represented either a full-size microscope field or n strips parallel to the motion with reduced height and n-fold increase of sampling frequency. After separating even and odd fields, the sampling frequency was thus $100 \times n$. It was possible to perform at least 200 position determinations per second with a computer endowed with a 80486 micropro-

cessor operated at 20 MHz frequency. The standard error of x-coordinate determination, as obtained by observing resting particles, was better than 0.2 pixel (Pierres et al., 1997). A typical trajectory consisted of 200–400 sets of position (including x and y coordinates, and particle area allowing to check the validity of analysis). A typical experiment yielded 50–100 trajectories corresponding to about 20,000 positions.

Under standard conditions, trajectories were processed for determination of the average velocity for a typical period of eight elementary steps (i.e., 160 ms—see below), and the average acceleration was derived from the velocity change during two sequential 160-ms intervals.

Direct determination of the wall shear rate

An approximate determination of the wall shear rate G was achieved by using the standard formula,

$$G = 6Q/wh^2, \tag{13}$$

were Q is the flow rate, and w and h are the chamber width and height, respectively. However, it was found that wide variations of G (sometimes higher than 40%) might occur on changing the chamber floor. This could be accounted for by variations of the chamber height, as evidenced by sequentially focusing on the upper and lower edge and using the micrometer screw of an Axiovert 135 (Zeiss) inverted microscope.

In some cases, direct determination of G was achieved by monitoring small spheres (1-μm diameter) with a 63× immersion length (to decrease the field depth) and measuring the displacement rate of typically 30 beads in sequential planes separated by equal intervals. Note that the actual distance e_a between these planes could be obtained with the micrometer scale of the microscope using the formula,

$$e_a = e_r n_w / n_o, \tag{14}$$

where e_r is the displacement of the objective (read on the micrometer scale), and n_o and n_w are the refractive index of oil and water, respectively (i.e., 1.50 and 1.33). Eq. 14 stems from the well-known property of a plate of refractive index n and thickness e to translate an image by $e(n - 1)/n$.

Computer simulation

All simulations were done with a Pentium-based (500 MHz) desk computer. The standard procedure consisted of starting 50 particles at varying height (usually between 50 and 100 nm from the surface). Each trajectory consisted of 800 steps of 20-ms duration. Each step was generated as a sequence of 100 "microsteps" of 0.2 ms each that were obtained following Eqs. 1–9. Simulated trajectories were studied with the same analysis software as was used to process experimental data.

In some cases, the rate of approach to equilibrium was studied by considering the local particle concentration c_i at height i and replacing stochastic jumps with deterministic variations,

$$\Delta c_i = [f_+(c_{i+1} - c_i) + f_-(c_{i-1} - c_i)]\Delta t. \tag{15}$$

RESULTS

Determining the optimal time step

Typical plots of particle position and velocity as functions of time are exemplified in Fig. 3, *A* and *B*. Random fluctuations in velocity are clearly evident when positions are measured over 40-ms intervals, but less severe when they are calculated over 160-ms intervals (Fig. 3, *C* and *D*). Velocity fluctuations reflect the Brownian motion rather than random measurement errors, because the measured velocity variations of stationary particles that adhered to the chamber floor are about fivefold smaller than those of freely moving particles (Fig. 3, *C* and *D*).

Similar randomly fluctuating velocities can be generated by simulations, which reveals that the particle-to-surface distance δ also appears as a random process (Fig. 4 *A*). Our goal is to relate δ to the measured velocity U. The presence of Brownian motions makes a deterministic relationship such as Eq. 5 impossible. Therefore, we want to derive the density distribution of δ from the average velocity in a given time interval Δt. The choice of Δt affects the correlation between δ and U. The time-step size was thus chosen to maximize this correlation. As shown in Fig. 4 *B*, the cross-correlation function achieves a maximum at $\Delta t \sim 0.1$ s. Indeed, the biphasic dependence of the cross-correlation on Δt reflects the effects of two competing requirements. First, Δt should be sufficiently small to limit the Brownian fluctuations in the z direction, the root mean square of which is $(2D_z\Delta t)^{1/2}$. Second, the averaged velocity U over Δt should be as close to the hydrodynamic velocity as possible. In other words, the ratio of the diffusive velocity $(D_z\Delta t)^{1/2}$ to u_h should be minimized. Based on the simulation results of Fig. 4, $\Delta t = 0.16$ s was used for measuring velocity and acceleration in experiments.

Relationship between acceleration and velocity

Previously, Pierres et al. (1998c) reported the use of an empirical relationship between the ensemble averages of particle acceleration and velocity to determine the shear rate and Hamaker constant. In the present work, we further investigated the theoretical basis of the acceleration versus

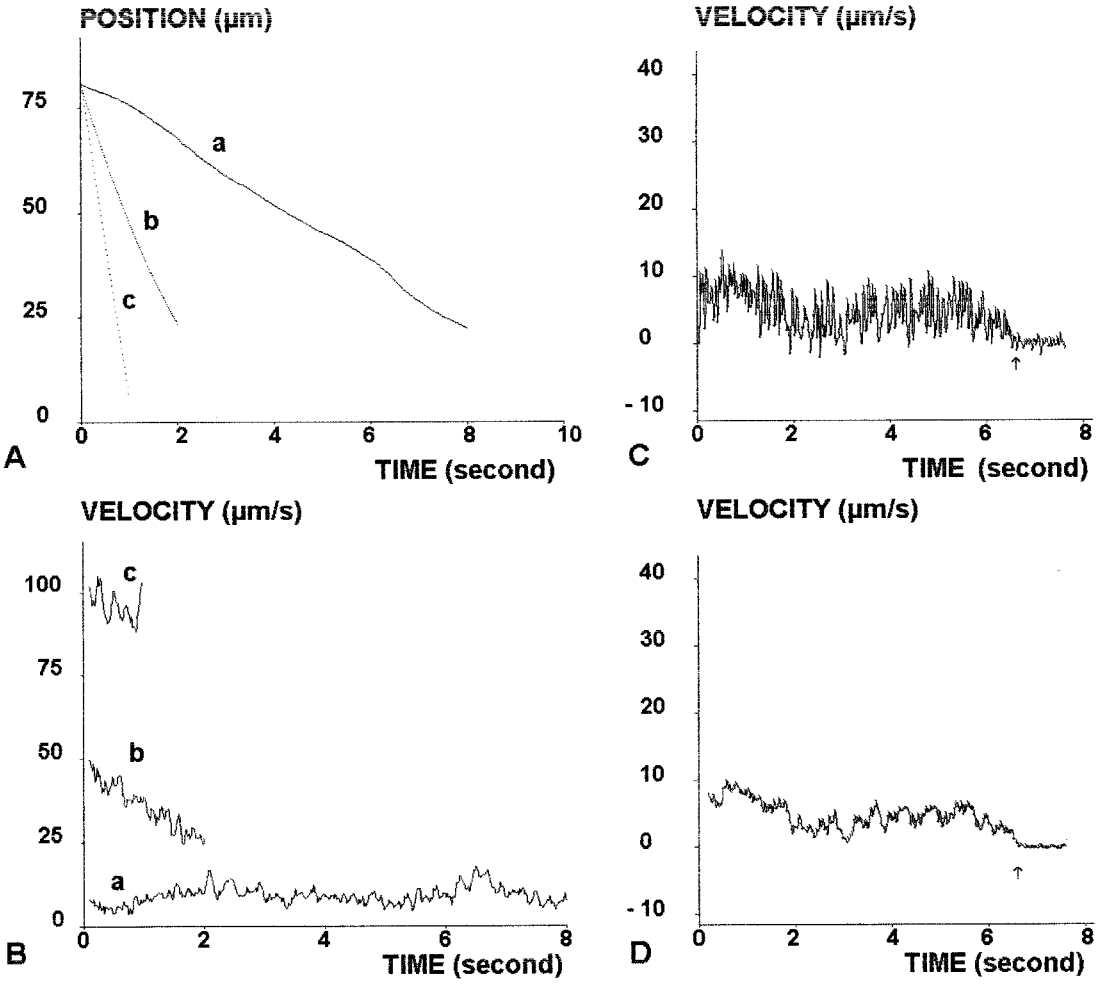

FIGURE 3 Representative trajectories. The motion of spheres of 2.8-μm diameter driven across a microscope field by a wall shear rate of 10–20 s^{-1} was monitored and the particle position was determined with a sampling frequency of 50 s^{-1}. (*A*) Three representative curves are shown. Particle (*a*) was close to the surface, whereas particles (*b*) and (*c*) had not completely sedimented. (*B*) Average velocities were calculated over 80-ms periods. Although all particles displayed random velocity fluctuations, sedimentation of particles (*b*) and (*c*) results in progressive velocity decrease. (*C*) The average velocity of a sphere moving along a biotin-derivatized surface was determined over 40 ms. An arrest is clearly visible (*arrow*) with immediate reduction of fluctuations. (*D*) Same as (*C*). Velocity is averaged over 160 ms.

velocity curve. In the absence of Brownian motion, the particle acceleration can be easily calculated:

$$\gamma_x = [du_h/dz][dz/dt] = \left[\frac{(0.011293 \ln^2(\delta/a) + 0.144664 \ln(\delta/a) + 0.54756)u_h}{\delta}\right]\left[\frac{-v_s}{F_z}\right], \quad (16)$$

where Eq. 5 has been used to calculate du_h/dz and F_z is given by Eq. 9. These predictions, which are based on the deterministic hydrodynamics (Fig. 5, *thick line*) clearly deviate from the experimental curve obtained by pooling 348 particle trajectories (Fig. 6, *open squares*). Thus, Eq. 16 predicts $\gamma_x < 0$ for all velocity values, yet positive accelerations were obtained at small velocities (Fig. 6). These discrepancies highlight the significance of the fluctuating velocities. Intuitively, due to the fluctuations along the x direction, when velocity is smaller than average in one instant, the odds for an even smaller velocity to occur in the next instant should be smaller than for a larger velocity to occur. Similarly, when a large velocity is observed, it is more likely to observe a smaller velocity than an even larger velocity the next time. This results in, on average, a negative correlation between acceleration and velocity. Likewise, the Brownian motion in the z direction should also contribute to the acceleration versus velocity curve (Eq. 12). This suggests that the acceleration versus velocity curve captures important statistical properties of the Brownian motion under consideration. Thus, to test our simulation algorithm for diffusive motions of Brownian spheres in a shear flow near

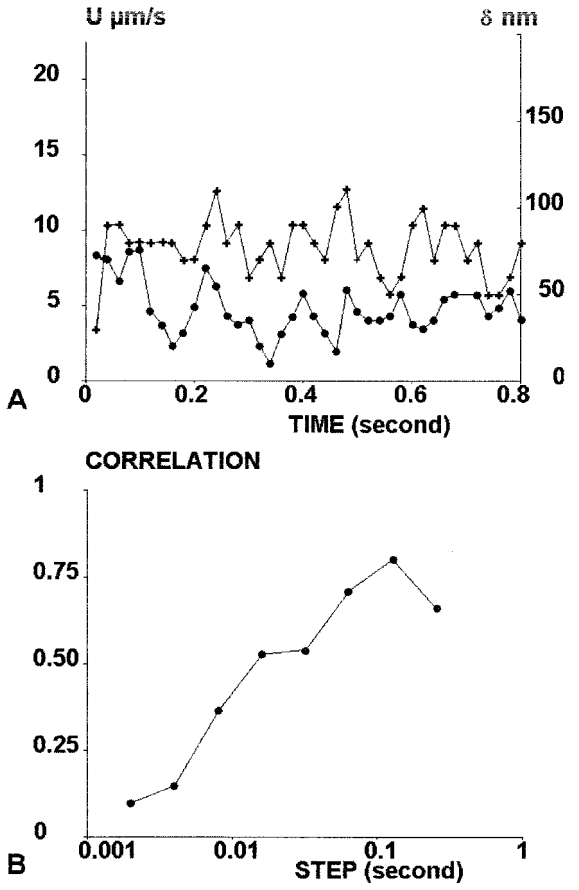

FIGURE 4 Tightness of correlation between particle velocity and distance to the wall. (*A*) The trajectory of a sphere (2.8-μm diameter) was simulated with elementary steps of 0.0001 s. Every 0.02 s, the particle distance to the wall (δ) and average velocity U during the previous 20 mss were recorded. The variations of parameters δ (*circles*, *right ordinate*) and U (*crosses*, *left ordinate*) during a period of 0.8 s are shown. (*B*) The correlation coefficient between particle distance to the surface and average velocity during a time step Δt was determined on simulated trajectories. The correlation was maximum for a time interval of order of 0.1 s.

a wall, simulated and measured acceleration versus velocity curves were carefully and systematically compared.

Four sets of simulations were performed with results shown in Fig. 5: without Brownian motions (*circles*), with Brownian motions in the x direction only (*diamonds*), with Brownian motions in the z direction only (*triangles*), and with Brownian motions in both x and z directions (*squares*). As expected, simulations in the absence of Brownian motions reproduce the deterministic relationship given by Eq. 16. The addition of Brownian motions in the z direction resulted in positive acceleration in the low-velocity regime. Inclusion of Brownian motions in both x and z directions yielded an acceleration curve in good agreement with experimental data (Fig. 6, *crosses*).

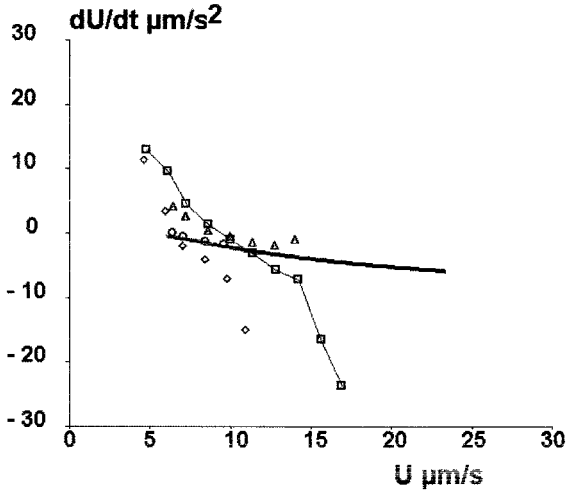

FIGURE 5 Physical significance of acceleration curves. The acceleration curve predicted by deterministic Goldman's theory (*continuous thick line*) is shown. Acceleration curves were also derived from simulated sets of trajectories that were built without any Brownian motion (*circles*), with Brownian motions along x axis only (*diamonds*) or along z axis only (*triangles*), or with Brownian motions along both x and z direction (*squares*).

In situ determination of the wall shear rate

We wish to determine the distribution of particle-to-surface distance z from the distribution of particle velocity. As will be discussed shortly, the probability $P_{U,\Delta t}(z)$ is highly sen-

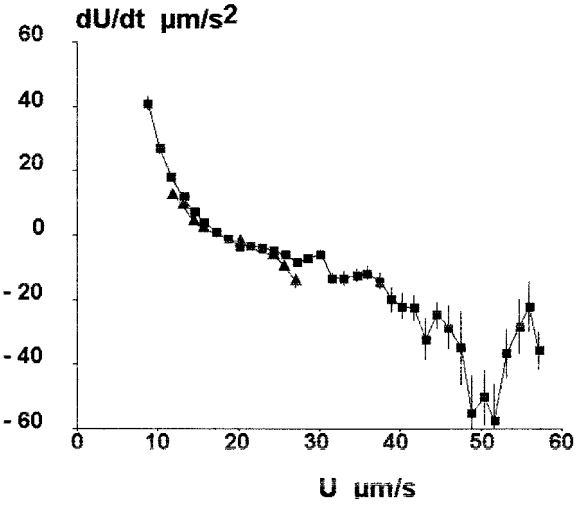

FIGURE 6 Acceleration curves comparing experimental and computed data. In a representative experiment, 348 spheres were monitored for determination of the acceleration curve (*squares*). Vertical bars represent standard error of the mean. The zero-acceleration velocity was 17.76 μm/s, yielding a wall shear rate of 18.8 s^{-1}. This value was used to simulate a series of 50 trajectories as explained. Simulated trajectories were processed similarly to experimental ones. The simulated acceleration curve (*triangles*) closely resembled the experimental ones in the region of interest, surrounding the zero-acceleration point.

sitive to the wall shear rate G. Although, in theory, G can be easily calculated from the flow rate and the chamber geometry, its experimental values were found to vary over a wide range (>40%) when the chamber floor was changed in repeated tests. This is due to uncontrollable variations in the chamber height despite that each time the flow chamber was reassembled carefully with identical screw turns. Therefore, a method is needed to precisely measure the wall shear rate in situ after the installation of the flow chamber. Our method is based on the dependence of the acceleration versus velocity curve on G, as determined by computer simulation. As shown in Fig. 7, numerical results suggest that the velocity U_0 corresponding to zero acceleration is proportional to the wall shear rate G. The coefficient of proportionality, 0.943 μm for the data shown, depends only weakly on the initial distribution of particle-to-surface distance, with the values being 0.954, 0.936, 0.498, 0.930, and 0.912 μm for five sets of particles (50 per set) initially located at δ = 20, 50, 100, 200, and 500 nm above the chamber floor. Thus, the wall shear rate can be determined in situ from the x-intercept of the measured particle acceleration curve.

The validity of the above method was tested by directly measuring the wall shear rate after 109 particle trajectories had been recorded. The microscope was then sequentially focused on planes located between 0 and 25 μm from the chamber, and the velocities of 30–40 particles in each focus plane were measured. As expected, the mean velocity of the particles was proportional to their distance from the chamber floor, allowing a value of G = 11.4 s^{-1} to be estimated from the slope of the line (Fig. 8). An independent G value of 12.2 s^{-1} was determined by using the method of acceleration curves, built by using the 109 particle trajectories recorded in the same chamber, which is in good agreement with the value measured directly.

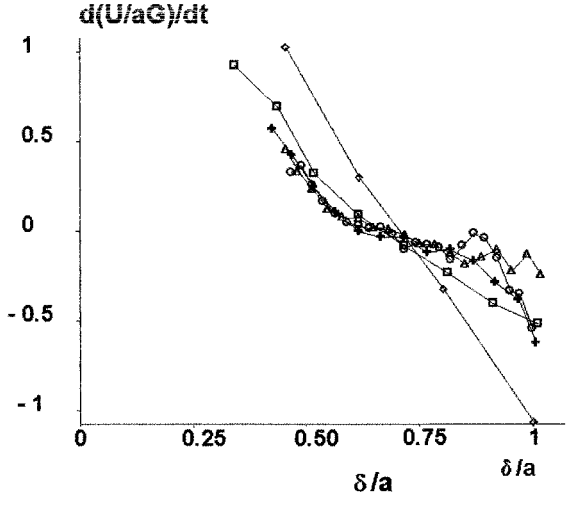

FIGURE 7 Dependence of acceleration curves on shear rate. Computer simulations were performed by generating a series of 50 random trajectories of 800 points at each G value, with an initial sphere-to-surface gap ranging between 50 and 100 nm. Acceleration was obtained by calculating the velocity difference between two sequential 160-ms intervals and plotted versus velocity for a wall shear rate of 5 (*diamonds*), 10 (*squares*), 20 (*crosses*), 30 (*triangles*) and 40 s^{-1} (*circles*). The velocity U_0 corresponding to no acceleration is close to 9.43 μm/s (U_0/aG = 0.67). Sphere radius a is 1.4 μm.

Effect of viscosity

We attribute the negative statistical correlation between acceleration and velocity as a property of Brownian motion.

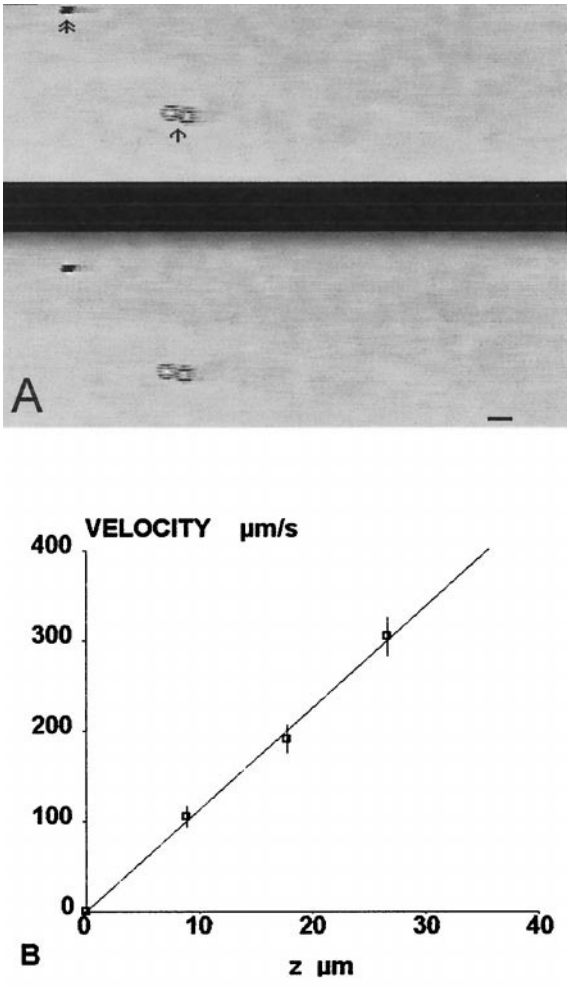

FIGURE 8 Direct determination of the wall shear rate. Spheres of micrometer size were subjected to a laminar shear flow in a double plate chamber. The microscope was sequentially focused on planes located away from the wall by increasing distances, as determined with the micrometer screw. The sphere velocity was determined by calculating the distance between two images corresponding to the two fields of each interlaced picture. (*A*) Two interlaced fields are separated by a 10-ms interval, horizontal bar length is 2.5 μm. Spheres that were located in the focus plane (*arrow*) were easily discriminated from those that were out-of-focus (*double arrow*). (*B*) The average velocity was determined on about 35 spheres in each plane, and mean values were plotted versus distance to the chamber floor. Vertical bar length is twice the standard deviation. The wall shear rate was calculated as the slope of the regression line.

This contention was tested by comparing the measured and predicted effects of the medium viscosity. Higher viscosity is expected to lower the contribution from the fluctuating velocity due to increased damping. This results in a broadened shallow region about U_0 in the acceleration versus velocity plot (Fig. 9). The agreement between experimental data and simulation also provides further support of our model.

Equilibrium distribution of particle heights in a quiescent fluid

At thermodynamic equilibrium, the particles should obey a Boltzmann distribution the expression of which can be obtained as the steady-state solution of Eq. 12:

$$n(z) = n_0 \exp(-z/h_B), \tag{17a}$$

where

$$h_B = k_B T/[(4/3)\pi a^3(\rho - \rho_w)g]. \tag{17b}$$

This general prediction from statistical mechanics provides us with a useful tool to check our model. Simulations were performed for particles of a radius of 1.4 μm and density of 1300 kg/m^3 (yielding h_B = 122 nm at room temperature) dispersed between two horizontal planes separated by a distance of 250 nm. The concentration profile was recorded after 20,000 elementary steps of 0.1 ms each. As shown in Fig. 10 *A*, excellent agreement was obtained between Eq. 17 and the simulated particle distribution.

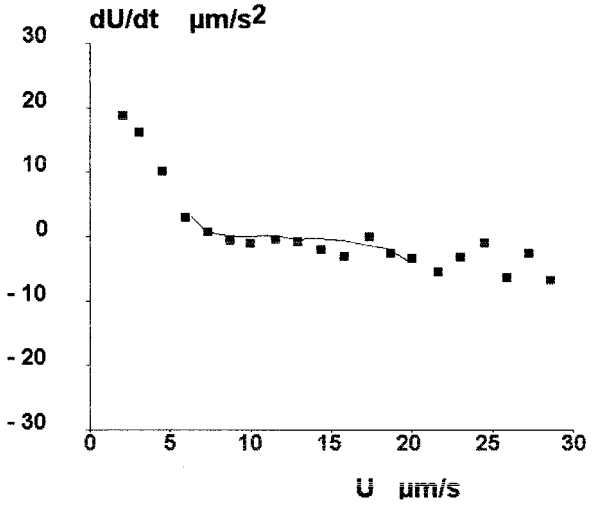

FIGURE 9 Effect of medium viscosity on acceleration plots. The motion of 39 spherical particles (1.4-μm radius) was studied in dextran solution with seven-fold increased viscosity as compared to water. The acceleration plot was determined and experimental data are shown (data) together with the simulated curve. Clearly, damping Brownian motion dramatically decreased the slope of the acceleration curve in the neighbourhood of $U = U_0$.

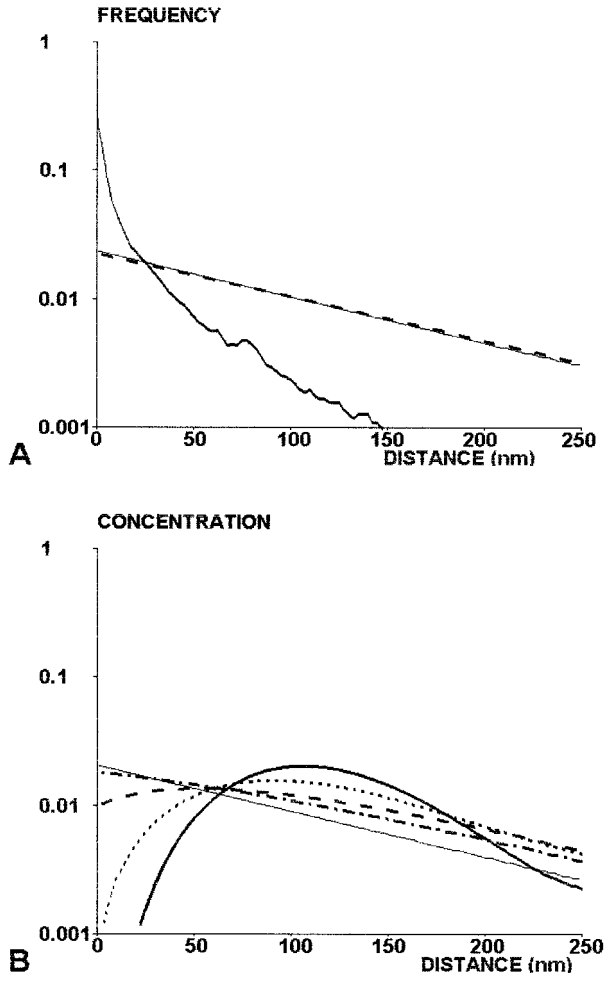

FIGURE 10 Simulation of the diffusion of an assembly of spheres near a wall. (*A*) Two different algorithms were used to simulate the Brownian diffusion of a sphere (1.4-μm radius, 1300-kg/m^3 density) perpendicularly to a wall in aqueous medium (0.001-Pa.s viscosity, 1000-kg/m^3 density). Standard Eqs. 1 and 2 were used to generate 1,000,000 random steps of 0.1 ms each. The diffusion coefficient was D^0/F_z, and the damping coefficient F_z was calculated with Eq. 9, using for the sphere-to-surface distance the instantaneous value preceding each step. The z distribution, as shown on thick continuous line, is markedly different from expected Boltzmann's distribution (thin continuous line). In contrast, a simulated distance distribution obtained with asymmetrical transition probabilities (*thick broken line*) closely matched Boltzmann's distribution. (*B*) A simulation was performed to study the diffusion of an assembly of buoyant spheres starting at 125-nm height in a region limited by two horizontal planes at 0 and 250-nm height. The concentration profile is shown after 1000 (*thick continuous line*), 2000 (*dotted line*), 5000 (*broken line*) and 10,000 (*dot-dash line*) steps of 0.1 ms. The equilibrium Boltzmann concentration is shown as a thin continuous line.

As discussed in the theoretical section, it was important to evaluate the diffusion coefficient $D_z(z)$ at the mid-value of each random displacement step in the simulation of diffusion in the z direction. Otherwise, the simulated equilibrium distribution will deviate from Boltzmann distribution. The verification of this contention is also shown on Fig. 10 *A*,

where the particle height distribution at 100 s (1,000,000 steps) simulated using drag coefficient $F_z(z)$ evaluated at the beginning of the step transition is plotted, which is evidently very different from the Boltzmann distribution.

It was interesting to determine the amount of time required for Boltzmann distribution to be obtained after dropping particles near a surface. As shown in Fig. 10 *B*, a minimum time of ~1 s was required to reach equilibrium.

Particle height distribution in a shear flow

The particle height distributions at given *U*/*aG* are exemplified in Fig. 11 *A*. These data were obtained by simulating the motion of a particle for a long period of 3200 s, with the *z* coordinate recorded every 0.1 ms and the velocity calculated every 160 ms. It is evident that $P_{U/aG,\Delta t}(z)$ is very sensitive to *U*/*aG*; thus, the mean height varies from ~20 to 41 nm when *U*/*aG* increases from 0.50 to 0.60. This emphasizes the importance of determining *G* with high accuracy. Also, the broad distributions shown on Fig. 11 *A* are consequences of Brownian motions, because the hydrodynamic theory predicts a single particle height for a given *U*/*aG* value.

Typical velocity histograms are shown in Fig. 11 *B*. The simulated particle trajectories give rise to a less scattered velocity distribution than that measured in the flow chamber, probably due to the broader distribution of initial particle heights in the experimental case. No attempt was made to extend the range of simulated velocities since the greater scattering of the experimental velocity histogram may be partly due to measurement errors.

The total probability distribution of particle heights in a representative experiment was calculated by combining the calculated conditional probability $P_{U/aG,\Delta t}(z)$ with the experimental velocity distribution. It is evident from Fig. 12 *A* that particle heights follow a Boltzmann distribution approximately when they are moving with the fluid with a nonzero hydrodynamic velocity u_h. As expected, such an equilibrium distribution does not depend on the medium viscosity despite the fact that both $P_{U/aG,\Delta t}(z)$ and particle velocity distribution change with viscosity and particle size (not shown). Also, when particles of a larger radius (2.25 μm, corresponding to $h_B = 29.5$ nm) were used, Boltzmann distribution was also obtained (Fig. 12).

The Boltzmann distribution is expected after the particles have achieved thermodynamic equilibrium. Deviations from Boltzmann distribution were observed, which were more severe near the wall, especially with particles of a larger radius and when they were moving in a more viscous fluid. That these discrepancies were due to incomplete sedimentation was confirmed by the next experiment. Here, particles were first delivered to the chamber and allowed to sediment in a quiescent, highly viscous fluid for 10 min before restarting the flow. As can be seen in Fig. 12 *B*, this resulted in an increased particle concentration near the chamber floor.

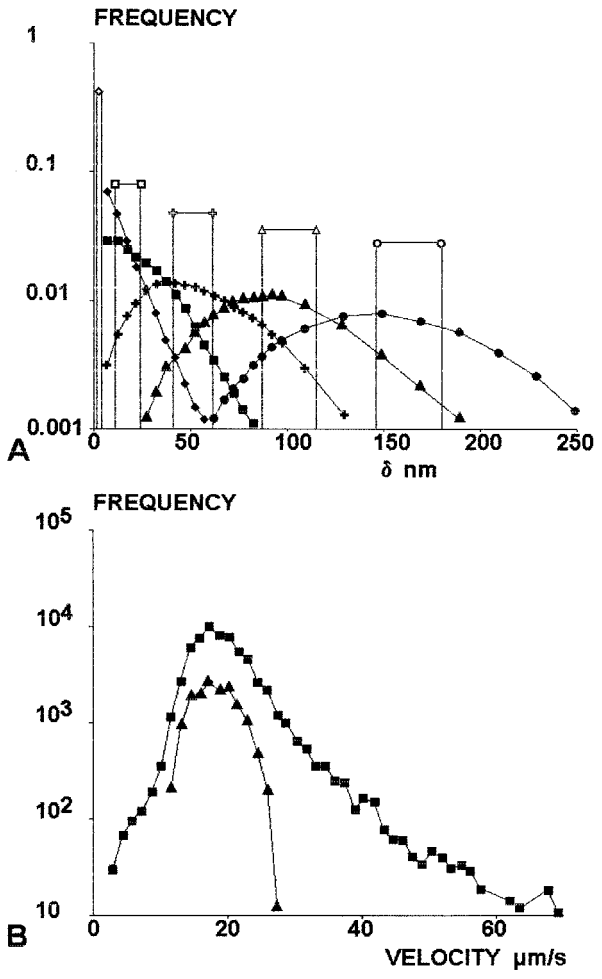

FIGURE 11 Relationship between sphere velocity and distance to the wall. (*A*) The trajectories of spherical particles subjected to a laminar shear flow with a wall shear rate 10 s^{-1} was simulated by generating 1.6×10^7 sequential steps of 0.1 ms each. The probability density of the sphere-to-surface distance δ was thus calculated as a function of the dimensionless velocity *U*/*aG* over a 160-ms time interval. Probabilities are shown when *U*/*aG* spans the following intervals: [0.40, 0.45[(*black diamonds*), [0.50, 0.55[(*black squares*), [0.60, 0.65[(*black crosses*), [0.70, 0.75[(*black triangles*), and [0.80, 0.85[(*black circles*). Rectangles (*open symbols*) represent the distribution obtained with deterministic Goldman's equations. The means (±SD) of the displayed distributions were respectively 13.8 + 8.3 nm, 20.5 + 14.6 nm, 41.2 + 25.2 nm, 77.6 + 34.5 nm, and 126.8 ± 43.9 nm. (*B*) Typical histograms of experimental (*squares*) and computed (*triangles*) velocity distributions are shown.

Influence of position measurement errors

The measurement errors may also contribute to the acceleration versus velocity curves. Because the acceleration at *t* is calculated as $[x(t + \Delta t) - 2x(t) + x(t - \Delta t)]/\Delta t^2$, an overestimated (or underestimated) value for $x(t)$ would lead to an underestimated (or overestimated) acceleration at *t*.

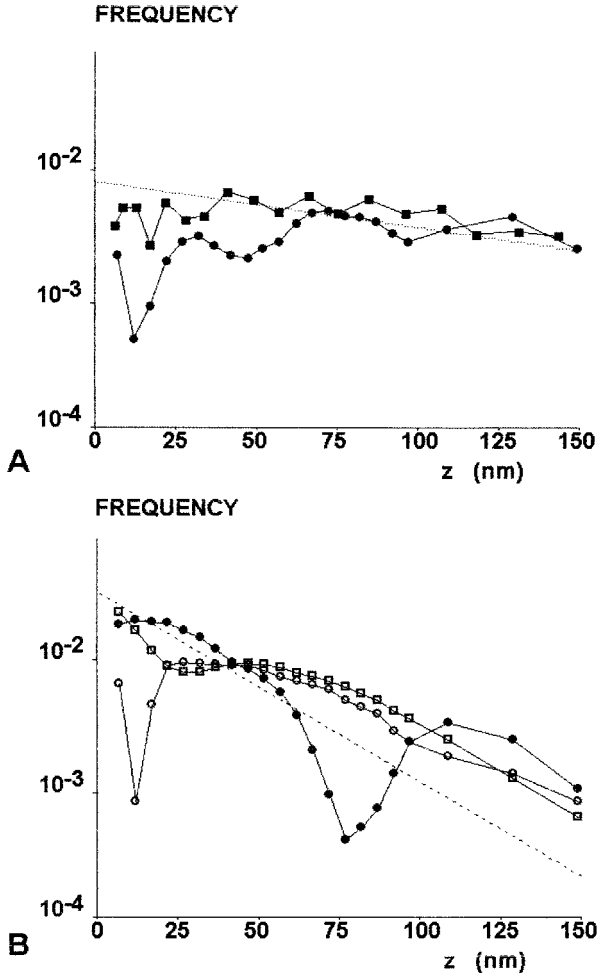

FIGURE 12 Distribution of sphere to surface distances. (*A*) In two representative experiments, series of spheres (1.4-μm radius) moving in normal aqueous (*squares*) or more viscous (sevenfold enhanced viscosity, *circles*) solution were monitored and velocity distribution was used to determine the distribution of z coordinates. The dotted line represents Boltzmann's distribution. The frequency of spheres closest to the wall is lower in viscous medium, in accordance with the expected decrease of sedimentation velocity. (*B*) Series of spheres (2.25 μm radius) moving in normal aqueous (*open squares*) or highly viscous (*open circles*) solution were monitored and the height density distribution is shown. The distribution obtained in highly viscous solution after 10 min equilibration is also shown (*black circles*).

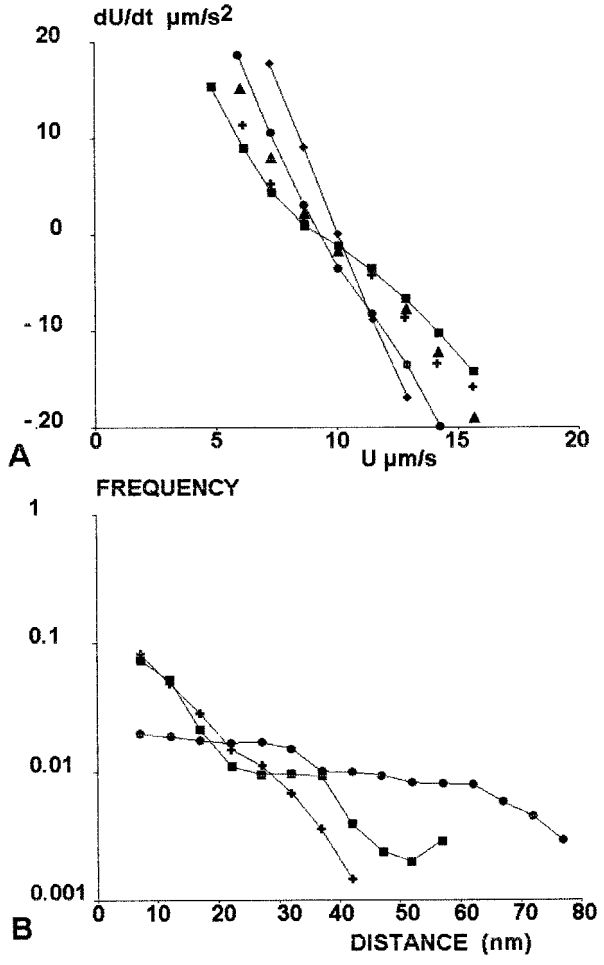

FIGURE 13 Effect of measurement error on the accuracy of sphere localization. (*A*) Series of trajectories of spheres subjected to a wall shear rate of 10 s^{-1} were simulated with addition of a normally distributed random error in position determination. Acceleration plots are shown with a root mean square error of 0 (*squares*), 44 nm (*crosses*), 100 nm (*triangles*), 150 nm (*circles*), and 250 nm (*diamonds*). (*B*) Simulations mentioned in Fig. 12 *A* were used to determine the probability density of distance δ to the wall as a function of average velocity U over 160-ms intervals. The distribution of δ is shown when U/aG is comprised between 0.35 and 0.40. The root-mean-square error in distance determination was, respectively, 0 (*crosses*), 44 nm (*squares*), and 250 nm (*circles*).

This also results in a negative correlation between acceleration and velocity. To determine such effects quantitatively, a normally distributed error with zero mean, and given standard deviation σ_x, was added in the simulations of displacement in the x direction. As shown in Fig. 13 *A*, addition of large measurement errors ($\sigma_x = 0.25$ μm) yielded a noticeable change in the acceleration versus velocity curve, resulting in a U_0/G ratio of 1.08 μm. However, measurement errors as small as those estimated from our experimental system (i.e., $\sigma_x = 0.044$ μm) showed minimal effects (Fig. 13 *A*).

The influence of position-measurement errors on the particle height distribution is shown in Fig. 12 *B*. Again, measurement errors with a standard deviation of 0.25 μm, but not those with $\sigma_x = 0.044$ μm, lead to a substantial change in $P_{U/aG,\Delta t}(z)$.

Estimate of the Hamaker constant

Simulations presented so far assumed no particle–surface interaction. In reality, van der Waals forces do exist, which may affect particle motion near the wall. As pointed by Pierres et al. (1998c), such weak interactions can be analyzed by using the acceleration versus velocity curve. In-

deed, because the sedimentation force in our experimental system is only ~34 fN, a method that allows accurate measurement of the sedimentation pattern and the change thereof should, in principle, enable detection of forces within the tens of femtonewton range. Using computer simulations, we explored the effect of van der Waals forces, $F = A_H a/(6\delta^2)$, on the particle motions. As shown in Fig. 14 *A*, particle height distribution is insensitive to the particle surface interactions in the range of the Hamaker constant A_H between 0 and 10^{-20} J. In comparison, the ratio U_0/G decreases with increasing A_H (Fig. 14 *B*). Thus, ignoring van der Waals forces may result in errors in the in situ determination of the wall shear rate. Conversely, combining our analysis with an independent measurement of the wall shear rate might allow for an accurate determination of the Hamaker constant. Because simulations with no particle–surface interaction produced acceleration versus velocity curves that matched the experimental data (Fig. 6) and estimated wall shear rates that were in good agreement with those measured independently, we conclude that van der Waals forces were negligible in our experimental system, as previously suggested (Pierres et al., 1998d).

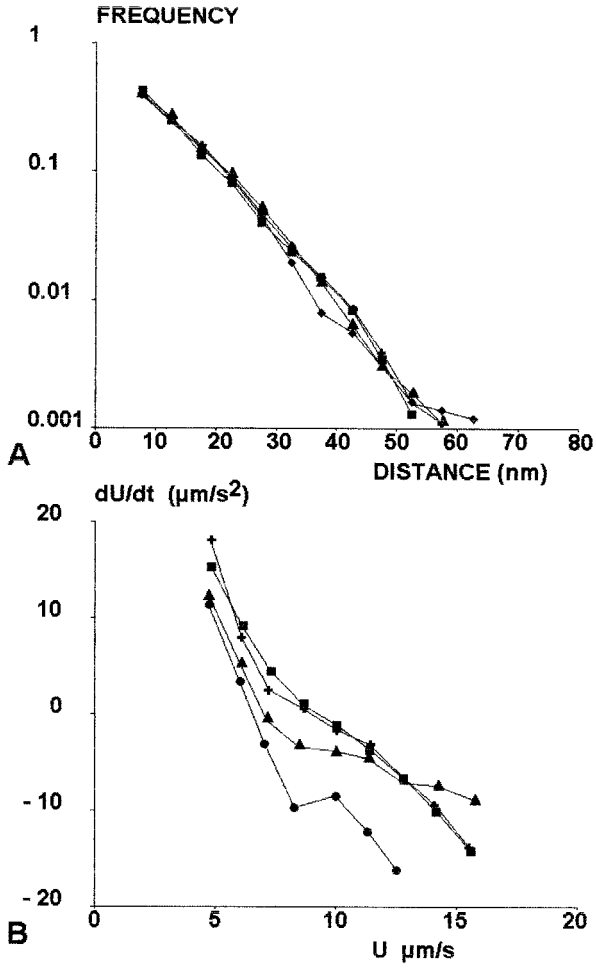

FIGURE 14 Influence of sphere to surface interaction on motion analysis. (*A*) Simulations were performed to generate a series of trajectories of spheres (1.4-μm radius) subjected to a wall shear rate of 20 s^{-1}. Sphere-to-surface interaction was described with a Hamaker constant of 0 (*crosses*), 10^{-22} (*squares*), 10^{-21} (*diamonds*), and 10^{-20} (*triangles*) Joule. The probability distribution of sphere-to-surface distance was determined when U/aG was between 0.4 and 0.5. Clearly, the relationship between apparent velocity and distance to the sphere was not strongly influenced by sphere-to-surface interaction. (*B*) Acceleration curves were generated by computer simulation using an Hamaker constant of 0 (*squares*), 0.02×10^{-20} (*crosses*), 0.07×10^{-20} (*triangles*) and 0.2×10^{-20} (*circles*) Joules. Clearly, the no-acceleration velocity U_0 was markedly influenced by van der Waals interactions, and the overall shape of acceleration curves was markedly altered when the Hamaker constant was 0.07×10^{-20} J or higher.

Importance of particle size and velocity

A final point was to determine the values of particle size and walls shear rate leading to optimal efficiency of our analysis. As exemplified in Fig. 15 *A*, increasing the wall shear rate might markedly improve the efficiency of particle-to-surface distance determination by reducing the relative importance of diffusion in horizontal displacement. However, this finding may be difficult to apply to the analysis of molecular interactions, because adhesion efficiency studied on many molecular models often displayed drastic decrease when particle velocity was increased.

Also, increasing particle size might decrease diffusion coefficients. As exemplified on Fig. 15 *B*, this results in better determination of z coordinate. However, because the force exerted on surface-bound particles is proportional to the square of the particle radius, increasing the particle radius might result in excessive disruptive force that might prevent adhesion.

CONCLUDING REMARKS

Computer simulation may be a powerful tool for deriving optimal information from experimental data. In the present work, we describe an algorithm allowing extensive analysis of the motion of buoyant Brownian spheres moving near a surface in the presence of a laminar shear flow and van der Waals forces. The main points of the study are 1) experimental check of the validity of our simulation, which can rarely be done with other models, 2) presented data provide an intuitive grasp of the motion, which is made very complicated by the combination of Brownian fluctuations and hydrodynamic interaction between particles and surface, 3) we emphasize the interest of studying the relationship between particle velocity and acceleration, which allows in situ determination of the wall shear rate and visualization of van der Waals forces, and 4) the importance of selectable parameters such as particle size and wall shear rate is analysed, and it is shown that recording the motion of micrometer-sized spheres with 0.1 second and 50 nm reso-

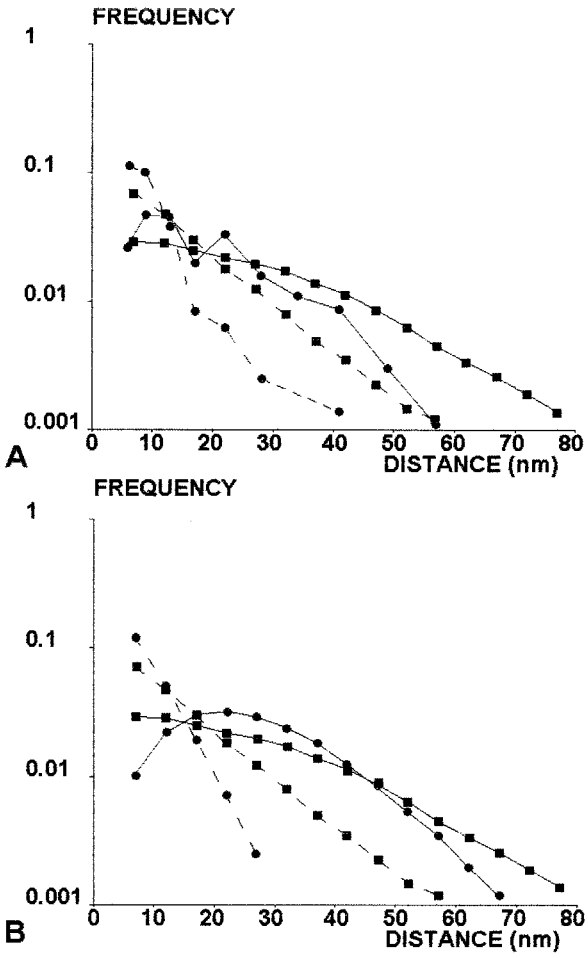

FIGURE 15 Dependence of velocity/distance relationship on basic parameters. (*A*) Simulations were performed to determine the sphere-to-surface distance distribution when U/aG was between 0.40 and 0.45 (*broken lines*) or 0.50 and 0.55 (*continuous lines*) and the wall shear rate was 10 s^{-1} (*squares*) or 20 s^{-1} (*circles*). The means and standard deviations of displayed distributions are, respectively, 13.8 ± 8.3 nm and 10.3 ± 6.3 nm (*broken lines*, 10 and 20 s^{-1}) and 20.5 ± 14.6 and 20.4 ± 12.3 nm (*continuous lines*, 10 and 20 s^{-1}). (*B*) The sphere-to-surface distance distribution was determined when the dimensionless velocity U/aG was between 0.40 and 0.45 (*broken lines*) or 0.50 and 0.55 (*continuous lines*) and the sphere radius was 1.4 μm (*squares*) or 2.25 μm (*circles*).

lution in presence of a hydrodynamic flow with a wall shear rate of ~10 s^{-1} allows one to monitor particle-to-surface distance within the 10-nm range and detect sphere-to-surface attraction with about 10 fN sensitivity.

First, our model allowed a fairly direct experimental check of our simulation algorithm. Indeed, it is often difficult to check completely the validity of computer simulations, because they often yield information that could not be obtained by a different method. The following tests were thus particularly useful:

1. Increasing the medium viscosity provided a simple way of damping particle diffusion, and complete aggreement between theoretical predictions and experimental acceleration curves provided a first check of the validity of our approach.
2. A more direct test was performed by showing that the derivation of the wall shear rate without the use of any fitted parameter yielded fairly accurate results.
3. Finally, the accordance between particle distribution and Boltzmann's law may be considered as satisfactory, because the lower-than-expected particle concentration near the surface may be accounted for by incomplete sedimentation.

Note that these experiments provided a quantitative test for the validity of both our simulation algorithm and Goldman's relationship between particle velocity and distance to the surface. Our conclusions are consistent with elegant experiments made by Georges et al. (1993) with an original surface force apparatus, suggesting that macroscopic flow equations remain valid when considered distances are higher than the size of solvent molecules (i.e., ~0.2-nm diameter for a water molecule).

Second, the curves shown on Fig. 10 *B* clarify the consequences of diffusive heterogeneity with respect to the approach to equilibrium. If particles are introduced in a bounded box, they will first concentrate toward regions where the diffusion coefficient is highest, resulting in nonuniform distribution. Then they spread more slowly toward regions of slow diffusion, until concentration is uniform. However, in a boundless region, particles will diffuse toward regions of high diffusion constant, until the concentration vanishes everywhere, thus resulting in an anisotropic flux that does not contradict thermodynamic principles because the final concentration is zero everywhere, and therefore is uniform.

Third, we demonstrated the interest in analyzing the relationship between average particle velocity and acceleration. Indeed, it was shown that a quantitative analysis of the plot obtained by pooling a few tens of thousands of position determinations allowed accurate determination of the wall shear rate (Fig. 7) and proper visualization of van der Waals interactions between particles and surface (Fig. 14). Indeed, because the sedimentation force was ~34 fN, accurate analysis of the particle sedimentation pattern, as captured by the velocity/acceleration plot, should clearly allow one to detect interactions in the tens of femtownewtons range. The absence of detectable interactions between particles and surfaces in our experimental model is consistent with the hypothesis that spheres might be coated by a low-density region (Pierres et al., 1998c,d) with a hydrodynamic surface at distance from the material surface. Indeed, a few polymer molecules may suffice to reduce water flow drastically (Wiegel, 1980). Because experiments were conducted in fairly concentrated electrolyte solutions (with a Debye Hückel length of order of 0.8 nm), van der Waals forces might play a dominant role in sphere-to-surface in-

teractions. Further, simulations demonstrated that, in addition to their theoretical importance, velocity/acceleration plots presented the important practical advantage of a weak dependence on particle-to-surface distance distribution. This is important, because this distribution is not generally known, and it may not be feasible to ensure that Boltzmann's distribution is followed in experimental models where significant particle-to-surface adhesion results in a net particle flux towards the surface.

Fourth, our numerical studies allow a quantitative assessment of the information that may be obtained on the rate of bond formation with a laminar flow chamber. According to our experience, efficient bond formation can be obtained by driving receptor-coated micrometer-sized particles along ligand-derivatized surfaces with a wall shear rate of $\sim 10\ s^{-1}$. The force acting on a single bond maintaining a particle at rest is then of order of only 5 pN (Pierres et al., 1996c), which may be low enough to result in minimal perturbation of the natural bond lifetime. As shown on Fig. 3 *C*, a particle stop of ~40 ms can be detected under these conditions. The required accuracy for position determination is about 50 nm (see also Fig. 13). This can be achieved by determining the center of the image of the spherical particle, but this could not be performed with living cells. In any case, the morphological irregularities of actual cells result in velocity fluctuations that preclude any detailed motion analysis. Finally, determining the experimental relationship between particle velocity and arrest probability will allow one to derive the distance dependence of adhesion efficiency by a deconvolution procedure relying on computed velocity/height relationship (Fig. 11 *A*). It is thus possible to study the formation of bonds resisting 5-pN force for 40 ms and study distance dependence of the on-rate with a resolution slightly better than 10 nm.

Therefore, the laminar flow chamber may be considered as the first (and perhaps the sole) method allowing direct study of adhesion frequency and distance-dependence between surface attached molecules (Pierres et al., 1997, 1998c). This is a complex process because this may involve both convection and diffusion effects (Chang and Hammer, 1999), which makes it difficult to relate 2D and 3D binding rates. Determining such relationship would be important to improve our understanding of the relationship between 2D association and dissociation rates, and affinity constants (Dustin, 1997). Further work is planned to address these problems with the flow chamber methodology.

APPENDIX: EFFECT OF SPHERE ROTATION ON TRANSLATIONAL MOTION

Two possible effects of sphere rotation may be considered: free rotation will reduce the translational friction coefficient, and random angular fluctuations will result in translational motion. The importance of both effects may be calculated with numerical results provided by Goldman et al. (1967a). The basis is to superimpose the following two motions:

Translation without rotation near a wall: A sphere moving with velocity U parallel to x axis is subjected by the fluid to a friction force F^T parallel to ωx and a torque T^T parallel to ωy,

$$F^T = -6\pi\mu a U F^{*T}, \tag{A1}$$

$$T^T = 8\pi\mu a^2 U T^{*T}, \tag{A2}$$

where starred symbols represent universal dimensionless coefficients that were determined numerically by Goldman et al. (1967a).

Rotation without translation near a wall: A sphere rotating with angular velocity Ω parallel to Oy (Fig. 1) is subjected by the fluid to a friction force F^R parallel to Ox and a torque T^R parallel to Oy,

$$F^R = 6\pi\mu a^2 \Omega, \tag{A3}$$

$$T^R = -8\pi\mu a^3 \Omega. \tag{A4}$$

Effect of rotation on the translational friction coefficient

Let us apply a force F parallel to Ox on a freely rotating sphere. The translational and rotational velocities U and Ω can be obtained with Eqs. A1–A4, by writing that the total hydrodynamic force is $-F$ and the torque is zero. We find

$$U = F/(6\pi\mu a F^{*T}[1 - F^{*R}T^{*T}/F^{*T}T^{*R}]). \tag{A5}$$

Thus, free rotation will increase the diffusion coefficient D_x, which is proportional to the reciprocal value of the friction coefficient F/U, by a factor $F^{*R}T^{*T}/F^{*T}T^{*R}$. Using the results provided by Goldman et al (1967a), it is found that this factor remains less than 1.8% when the nondimensional distance δ/a between the sphere and the wall is higher than 0.0032.

Effect of random rotation on translation

There is another effect of sphere rotation on translational diffusion. Using the same kind of reasoning as above, we find that a freely translating sphere with angular velocity Ω parallel to ωx will acquire a translational velocity $U = aF^{*R}/F^{*T}$ parallel to Ox. Because the translational and rotational diffusion coefficients D_x and $D_{\omega y}$ are proportional to the square of random displacement during a given time interval, it may be shown that rotational diffusion of a freely translating sphere will increase the translational diffusion coefficient D_x by the value

$$\Delta D_x = (aF^{*R}/F^{*T})^2 D_{\omega y}. \tag{A6}$$

The rotational friction coefficient can be obtained with Eqs. A1–A4, using the same procedure as was used for the translational diffusion coefficient. Finally, we find that free rotation will increase D_x by a relative amount of

$$6/8(F^{*R}/F^{*T})^2 \times F^{*T}[1 - F^{*R}T^{*T}/F^{*T}T^{*R}]. \tag{A7}$$

Using the numerical data provided by Goldman et al. (1967b), we find that the relative increase of D_x remains lower than 0.06 when δ/a is higher than 0.0032.

The expert technical assistance of Ms. Dominique Touchard is gratefully acknowledged. P.B. is indebted to Drs. Jacques Prost and Pierre Schaaf for helpful discussions. C.Z. acknowledges the support of National Institutes of Health grants AI38282 and AI44902 and INSERM "Poste Orange." This work was supported by a grant from the "Bioinformatics" program.

REFERENCES

Alon, R., D. A. Hammer, and T. A. Springer. 1995. Lifetime of P-selectin-carbohydrate bond and its response to tensile force in hydrodynamic flow. *Nature.* 374:539–542.

Alon, R., S. Chen, K. D. Puri, E. B. Finger, and T. A. Springer. 1997. The kinetics of L-selectin tethers and the mechanics of selectin-mediated rolling. *J. Cell Biol.* 138:1169–1180.

Baumgartner, W., P. Hinterdorfer, W. Ness, A. Raab, D. Vestweber, H. Schindler, and D. Drenchahn. 2000. Cadherin interaction probed by atomic force microscopy. *Proc. Natl. Acad. Sci. U.S.A.* 97:4005–4010.

Bell, G. I. 1978. Models for the specific adhesion of cells to cells. *Science.* 200:618–627.

Benoliel, A. M., C. Capo, J. L. Mège, and P. Bongrand. 1994. Measurement of the strength of cell–cell and cell–substratum adhesion with simple methods. *In* Studying Cell Adhesion. P. Bongrand, P. Claesson, and A. Curtis, editors. Springer Verlag, Heidelberg, Germany. 81–92.

Brenner, H. 1961. The slow motion of a sphere through a viscous fluid towards a plane surface. *Chem. Engn. Sci.* 16:242–251.

Brune, D., and S. Kim. 1994. Hydrodynamic steering effects in protein association. *Proc. Natl. Acad. Sci. U.S.A.* 91:2930–2934.

Chang, K. C., and D. A. Hammer. 1999. The forward rate of binding of surface-tethered reactants: effects of relative motion between two surfaces. *Biophys. J.* 73:1280–1292.

Chen S., R. Alon, R. C. Fuhlbrigge, and T. A. Springer. 1997. Rolling and transient tethering of leukocytes on antibodies reveal specializations of selectins. *Proc. Natl. Acad. Sci. U.S.A.* 94:3172–3177.

Chen, S. and T. A. Springer. 1999. An automatic braking system that stabilizes leukocyte rolling by an increase in selectin bond number with shear. *J. Cell Biol.* 94:195–200.

Chesla, S. E., P. Li, S. Nagarajan, P. Selvaraj, and C. Jhu. 2000. The membrane anchor influences ligand binding two-dimensional kinetic rates and three-dimensional affinity of FCγ RIII (CD16). *J. Biol. Chem.* 275:10235–10246.

Chesla, S. E., P. Selvaraj, and C. Zhu. 1998. Measuring two-dimensional receptor–ligand binding kinetics by micropipette. *Biophys. J.* 75: 1553–1572.

Dimitrov, D. S. 1983. Dynamic interactions between approaching surfaces of biological interest. *Prog. Surface Sci.* 14:295–423.

Dustin, M. L., L. M. Ferguson, P. Y. Chan, T. A. Springer, and D. E. Golan. 1996. Visualization of CD2 interaction with LFA-3 and determination of the two-dimensional dissociation constant for adhesion receptors in a contact area. *J. Cell Biol.* 132:465–474.

Dustin, M. L. 1997. Adhesive bond dynamics in contacts between T lymphocytes and glass-supported planar bilayers reconstituted with the immunoglobulin-related adhesion molecule CD58. *J. Biol. Chem.* 272: 15782–15788.

Ermak, D. L., and J. A. McCammon. 1978. Brownian dynamics with hydrodynamic interactions. *J. Chem. Phys.* 69:1352–1360.

Evans, E., and K. Ritchie. 1997. Dynamic strength of molecular adhesion bonds. *Biophys. J.* 72:1541–1555.

Fritz, J., A. G. Katopodis, F. Kollinger, and D. Anselmetti. 1998. Force-mediated kinetics of single P-selectin/ligand complexes observed by atomic force microscopy. *Proc. Natl. Acad. Sci. U.S.A.* 95:12283–12288.

Gabdouline, R. R., and R. C. Wade. 1997. Simulation of the diffusional association of barnase and barnstar. *Biophys. J.* 72:1917–1929.

Georges, J. M., S. Millot, J. L. Loubet, and A. Tonck. 1993. Drainage of thin liquid films between relatively smooth surfaces. *J. Chem. Phys.* 98:7345–7360.

Goldman, A. J., R. G. Cox, and H. Brenner. 1967a. Slow viscous motion of a sphere parallel to a plane wall. I. Motion through a quiescent fluid. *Chem. Engn. Sci.* 22:637–651.

Goldman, A. J., R. G. Cox, and H. Brenner. 1967b. Slow viscous motion of a sphere parallel to a plane wall. II. Couette flow. *Chem. Engn. Sci.* 22:653–660.

Happel, J., and H. Brenner. 1991. Low Reynolds Number Hydrodynamics. Kluwer Academic Publishers, Dordrecht, The Netherlands.

Hinterdorfer, P., W. Baumgartner, H. J. Gruber, K. Schilcher, and H. Schindler. 1996. Detection and localization of individual antibody–antigen recognition events by atomic force microscopy. *Proc. Natl. Acad. Sci. U.S.A.* 93:3477–3481.

Israelachvili, J. N. 1991. Intermolecular and Surface Forces. Academic Press, New York.

Kaplanski, G., C. Farnarier, O. Tissot, A. Pierres, A. M. Benoliel, M. C. Alessi, S. Kaplanski, and P. Bongrand. 1993. Granulocyte–endothelium initial adhesion. Analysis of transient binding events mediated by E-selectin in a laminar shear flow. *Biophys. J.* 64:1922–1933.

Labadia, M. E., D. D. Jeanfavre, G. O. Caviness, and M. M. Morelock. 1998. Molecular regulation of the interaction between leukocyte-function-associated antigen-1 and soluble ICAM-1 by divalent metal cations. *J. Immunol.* 161:836–842.

Mehta, P., R. D. Cummings, and R. P. McEver. 1998. Affinity and kinetic analysis of P-selectin binding to P-selectin glycoprotein ligand-1. *J. Biol. Chem.* 273:32506–32513.

Nieba, L., A. Krebber, and A. Plückthun. 1996. Competition BIAcore for measuring true affinities: large differences from values determined from binding kinetics. *Anal. Biochem.* 234:155–165.

Pierres, A., A. M. Benoliel, and P. Bongrand. 1995. Measuring the lifetime of bonds made between surface-linked molecules. *J. Biol. Chem.* 270: 26586–26592.

Pierres, A., A. M. Benoliel, P. Bongrand, and P. A. van der Merwe. 1996a. Determination of the lifetime and force dependence of interactions of single bonds between surface-attached CD2 and CD48 adhesion molecules. *Proc. Natl. Acad. Sci. U.S.A.* 93:15114–15118.

Pierres, A., A. M. Benoliel, and P. Bongrand. 1996b. Measuring bonds between surface-associated molecules. *J. Immunol. Meth.* 196:105–120.

Pierres, A., A. M. Benoliel, and P. Bongrand. 1996c. Experimental study of the rate of bond formation between individual receptor-coated spheres and ligand-bearing surfaces. *J. Physique III.* 6:807–824.

Pierres, A., A. M. Benoliel, and P. Bongrand. 1997. The dependence of the association-rate of surface-attached adhesion molecules CD2 and CD48 on separation distance. *FEBS Lett.* 403:239–244.

Pierres, A., A. M. Benoliel, and P. Bongrand. 1998a. Interactions between biological sufaces. *Curr. Opin. Colloid Interface Sci.* 3:525–533.

Pierres, A., A. M. Benoliel, and P. Bongrand. 1998b. Studying receptor-mediated cell adhesion at the single molecule level. *Cell Adhesion Commun.* 5:375–395.

Pierres, A., H. Feracci, V. Delmas, A. M. Benoliel, J. P. Thiéry, and P. Bongrand. 1998c. Experimental study of the interaction range and association rate of surface-attached cadherin 11. *Proc. Natl. Acad. Sci. U.S.A.* 95:9256–9261.

Pierres, A., A. M. Benoliel, and P. Bongrand. 1998d. Use of a laminar flow chamber to study the rate of bond formation and dissociation between surface-bound adhesion molecules: effect of applied force and distance between surfaces. *Faraday Disc.* 111:321–330.

Ramachandran, V., M. U. Nollert, H. Qiu, W. J. Liu, R. D. Cummings, C. Zhu, and R. P. McEver. 1999. Tyrosine replacement in P-selectin glycoprotein ligand-1 affects distinct kinetic and mechanical properties of bonds with P- and L-selectin. *Proc. Natl. Acad. Sci. U.S.A.* 96: 13771–13776.

Risken, H. 1989. The Fokker–Planck Equation. Springer Verlag, Berlin.

Rossky, P. J., J. D. Doll, and H. L. Friedman. 1978. Brownian dynamics as smart Monte Carlo simulation. *J. Chem. Phys.* 69:4628–4633.

Schuck, P. 1997. Use of surface plasmon resonance to probe the equilibrium and dynamic aspects of interactions between biological macromolecules. *Ann. Rev. Biophys. Biomol. Struct.* 26:541–566.

Smith, M. J., E. L. Berg, and M. B. Lawrence. 1999. A direct comparison of selectin-mediated transient, adhesive events using high temporal resolution. *Biophys. J.* 77:3371–3383.

van der Merwe, P. A., M. H. Brown, S. J. Davis, and A. N. Barclay. 1993. Affinity and kinetic analysis of the interaction of the cell adhesion molecules rat CD2 and CD48. *EMBO J.* 12:4945–4954.

van Kampen, N. G. 1981. Stochastic Processes in Physics and Chemistry. North-Holland, Amsterdam.

Wiegel, F. W. 1980. Fluid Flow through Porous Macromolecular Systems. Springer Verlag, Berlin.

Williams, T. E., P. Selvaraj, and C. Zhu. 2000a. Concurrent binding to multiple ligands: kinetic rates of CD16b for membrane-bound IgG1 and IgG2. *Biophys. J.* 79:1850–1866.

Williams, T. E., S. Nagarajan, P. Selvaraj, and C. Zhu. 2000b. Concurrent and independent binding of Fcγ receptors IIa and IIIb to surface-bound IgG. *Biophys. J.* 79:1867–1875.

Wilcox, B. E., G. F. Gao, J. R. Wyer, J. E. Ladbury, J. I. Bell, B. K. Jacobsen, and P. A. van der Merwe. 1999. TCR binding to peptide-MHC stabilizes a flexible recognition interface. *Immunity*. 10: 357–365.

Zhu, C. 2000. Kinetics and mechanics of cell adhesion. *J. Biomech.* 33:23–33.